

Candidate platform for studying flatband-induced spin-triplet superconductivity

P. Sidorczak^{1,2,3,*}, W. Wołkanowicz⁴, A. Kaleta⁴, M. Wójcik⁴, S. Gieraltowska⁴, K. Gas^{4,6}, T. Płociński⁵, R. Minikayev⁴, S. Kret⁴, M. Sawicki^{4,7}, T. Wojtowicz², D. Wasik¹, M. Gryglas-Borysiewicz^{1,†} and K. Dybko^{2,4‡}

¹*Faculty of Physics, University of Warsaw, ul. Pasteura 5, 02-093, Warsaw, Poland*

²*International Research Centre MagTop, Institute of Physics,*

Polish Academy of Sciences, al. Lotników 32/46, 02668, Warsaw, Poland

³*Center for Quantum Devices, Niels Bohr Institute,*

University of Copenhagen, Universitetsparken 5, 2100 Copenhagen, Denmark

⁴*Institute of Physics, Polish Academy of Sciences, al. Lotników 32/46, 02668, Warsaw, Poland*

⁵*Faculty of Materials Science and Engineering, Warsaw University of Technology, Woloska 141, 02-507, Warsaw, Poland*

⁶*Center for Science and Innovation in Spintronics, Tohoku University,*

Katahira 2-1-1, Aoba-ku, Sendai 980-8577, Japan and

⁷*Research Institute of Electrical Communication, Tohoku University,*

Katahira 2-1-1, Aoba-ku, Sendai 980-8577, Japan

(Dated: June 6, 2024)

This paper explores the potential for spin-triplet superconductivity in molecular beam epitaxy-grown IV-VI semiconductor superlattices. The findings present compelling evidence for spin-triplet pairing in PbTe/SnTe by the method of soft point-contact spectroscopy and spin-polarised point-contact spectroscopy. The experimental data are understood with the Anderson-Brinkman-Morel model of p-wave electron pairing. It is pointed out that emergent superconductivity can have its origin in topological flat bands obtained due to internal stresses of the sample similar to twisted layer graphene.

The search for spin-triplet superconductors is propelled by their potential applications in spintronics and quantum computation [1–8]. It is predicted that these superconductors (SCs) host Majorana fermions at their boundaries. Recent breakthroughs in twisted bi-layer graphene experiments have unveiled signatures of spin-triplet superconductivity at specific "magic angles" [9, 10], due to strain-induced electron flatbands. The exploration of a flatband regime presents exciting possibilities for engineering high- T_c superconductors [11–13]. Additionally, intriguing results have surfaced in heavy fermion compounds [14, 15] and unconventional materials like $K_2Cr_3As_3$ [16], challenging the conventional understanding of superconductivity. Sr_2RuO_4 , once believed to be the sole confirmed case of a triplet superconductor, has faced recent reinterpretation [17, 18]. Proximity-induced spin-triplet superconductivity, involving injecting spin-singlet Cooper pairs into a medium with ferromagnetism or spin-orbit coupling, has also been explored [19–21].

Our study focuses on a different superconducting system: IV-VI semiconductor superlattices. In the early studies of those systems, the crucial role of the periodic dislocation grid was identified [22–28]. However, to our knowledge, the type of the superconducting pairing symmetry has not been established up to now. The revival of this topic came with the theoretical paper by Tang and Fu [29]. They linked the local band inversion to the strain in the periodic dislocation grid, which results in the topological crystalline insulator phase [30]. The periodically varying strain gives rise to flatbands which promote the superconducting state, predicted to show non-Bardeen-Cooper-Schrieffer (BCS) behaviour. A similar flatband system was present in super-

fluid 3He , where p-wave symmetry of the Cooper pairs has been identified [31–33].

Here we exploit point-contact spectroscopy of PbTe/SnTe superlattices to determine the pairing symmetry of the strain-induced superconductivity. Our investigations were motivated by encouraging results of spin polarized point-contact spectroscopy (spin-polarized PCS), which pointed to spin-triplet symmetry. Systematic studies of differential conductance spectra were performed on a series of samples as a function of temperature and magnetic field. All the spectra revealed zero bias conductance peak (ZBCP), expected for the unconventional superconductivity. The results are consistent with the Anderson-Brinkman-Morel (ABM) anisotropic p-wave superconductor model [34–38]. This model comes from the most understood case of spin-triplet pairing - superfluid 3He [39, 40]. Basic parameters of the superconducting state were extracted from resistance dependence on temperature and magnetic field, $R(T, H)$, pointing to its two-dimensional character, as predicted by Tang and Fu [23–25, 29].

Our PbTe/SnTe semiconductor heterostructures are grown by molecular beam epitaxy (MBE) on a $4\mu m$ thick CdTe buffer layer on semi-insulating GaAs and KCl substrates oriented in [100] direction. A two-dimensional mode of growth has been confirmed by streaky reflection high energy electron diffraction (RHEED) patterns. Lattice mismatch between 2 consecutive semiconductors leads to the formation of a periodic dislocation grid at the interface. It is visualised in Figure 1a) using the Bright Field transmission electron microscope (TEM) imaging condition obtained near [110] axis. Moreover, we underline that the Z-contrast STEM shows the layers to be almost fully relaxed far from the interfaces and that no extended defects in the form of threading dislocations or stacking faults crossing the whole heterostructure are present. Heterostructures with up to 7 semiconductor layers were studied. Collection of the extended RHEED, X-ray diffraction, and TEM

* pawel.sidorczak@nbi.ku.dk

† Marta.Gryglas@fuw.edu.pl

‡ dybko@ifpan.edu.pl

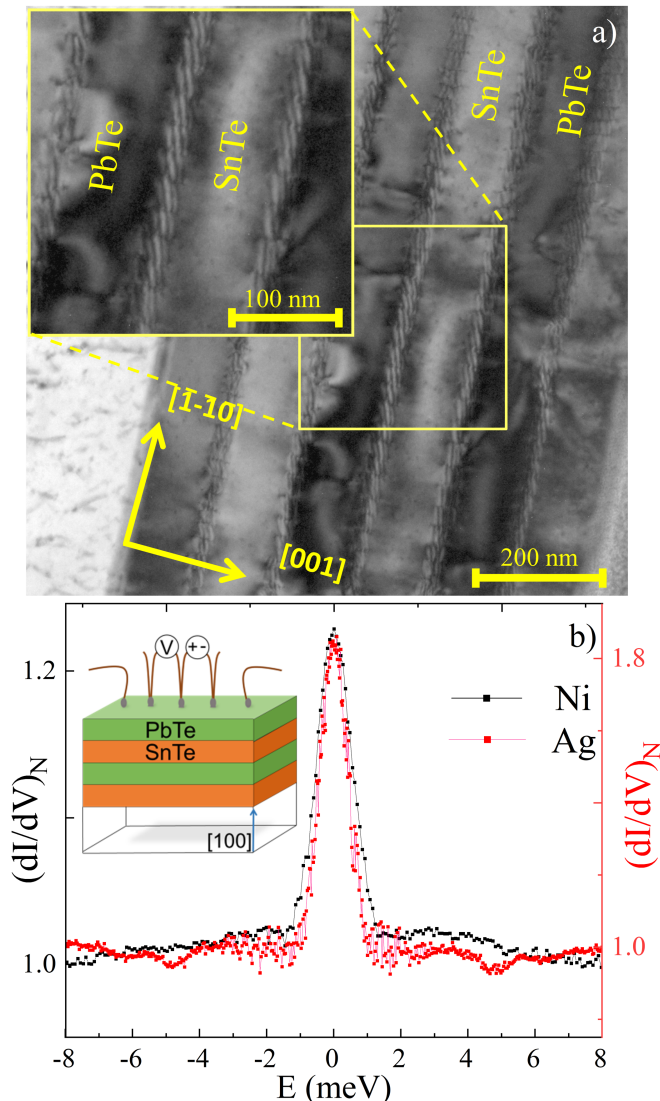


FIG. 1. a) TEM image of the cross-section of PbTe/SnTe superlattice. The alternating streaks along layer's interfaces mark periodic dislocation grid. b) Normalised dI/dV spectra measured with both nickel ($P_{Ni} \approx 44\%$) paste and silver ($P_{Ag} \approx 0\%$) paste contacts at $T = 1.8$ K. Spin polarised current preserves Andreev ZBCP, which is a fingerprint of spin-triplet SC. Insert: Scheme of experimental setup used for investigation of soft PCS.

characterisation is presented in the Supplemental Material [41] Figs. S1-S2.

Point-contact spectroscopy is an experimental technique involving the Andreev reflection (or tunnelling) of an electron on the interface between a superconductor and a normal metal. This is a process in which a single electron with momentum k is injected into a superconductor and binds with a free electron forming a Cooper pair. Since the momentum, spin, and number of particles are conserved a single hole is reflected with momentum equal to $-k$ and an adequate spin [42]. This process can be studied by measuring differential conductance as a function of the voltage bias V corresponding to incident electron energy (eV), schematically shown in the insert to Fig.1b). This technique allows us to study the SC order parameter Δ and to distinguish between different orbital symmetries (s-wave, p-wave, d-

wave)[43].

In this work soft PCS is employed, which means that instead of using a hard metallic tip contact (hard PCS), a metallic (usually silver) paste is used [42, 43]. This technique allows for an accessible approach to PCS, with the only drawback that the contact cannot be controlled in situ (see also Supplemental Material [41] Fig. S3 for more details). The results of PCS revealed that the spectra consist of a single zero-bias conductance peak (ZBCP) together with symmetric dips on the sides. Remarkably, such a result is independent of spin polarisation P , as shown in Fig.1b). This property of the PCS is a fingerprint of a spin-triplet SC (another example is Fig. S4 in Supplemental Material[41]). As quoted above, for the Andreev reflection to occur, there needs to be a hole available in the emitter with adequate spin in relation to the incident electron: opposite (singlet pairing) or identical (triplet pairing). If a current is injected to the SC via spin polarised contact, such as a ferromagnetic metal, the above condition will only be fulfilled for a spin-triplet superconductor [34]. In our case, the spectra are qualitatively identical, differing only in amplitudes. The latter can be ascribed to various grain sizes of the silver and nickel paste, distinct broadening parameters, and variations in the Fermi energy between silver and nickel. Moreover, as shown in Supplemental Material Fig. S5, we exclude the possibility that ZBCP is due to either the thermal regime of the point-contact or the Josephson junction coupling between superconducting domains [42, 45].

The above result is clear, qualitative proof of unconventional superconductivity in PbTe/SnTe superlattices. To gain more insight, the differential conductance spectra are analyzed with the model calculated for normal metal/ABM p-wave superconductor junction with a 4-component wave function [34, 46, 47]. Such a system can be characterised by the following parameters: Δ - order parameter, Z - transparency of a δ -like barrier between the SC and normal metal, Γ - inelastic scattering factor, and ϕ - the angle describing the relative position of the nodal points of the ABM model and the interface.

Experimental results of point-contact spectroscopy as a function of temperature for 2 different samples are presented in Fig. 2a) and b). The data are fitted with the theoretical model mentioned above. The fit parameters are listed in the Supplemental Materials [41] in Fig. S6. The model reproduces the data very well. The most external dips, marked on Fig. 2b) and attributed to the critical current [44], were not taken into account due to limitations of the model. The spectra are smoother and have more easily distinguished features than the ones presented in Fig. 1. We attribute this fact to the presence of a varying size of the superconducting island-like regions identified in Ref. [26].

Values of Δ obtained from the ABM fit in Fig. 2a) and b) are presented in panels c) and d), respectively. Solid lines are obtained from a simplified BCS formula [48]:

$$\Delta(T) = \Delta_{T=0} \left(1 - \left(\frac{T}{T_c} \right)^{3.2} \right)^{0.5}, \quad (1)$$

where $\Delta_{T=0}$ is the SC order parameter Δ at absolute zero.

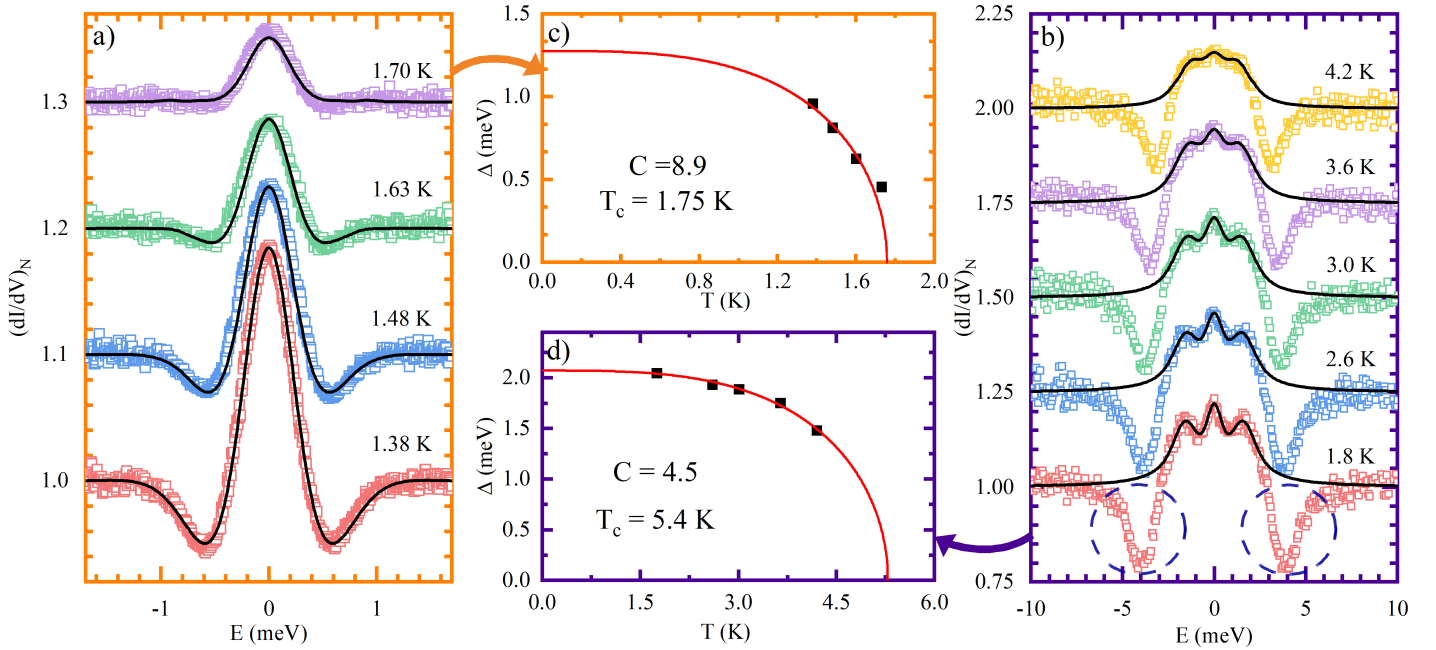


FIG. 2. a,b) Normalised PCS results obtained for 2 samples fitted with the ABM model. Dips at $E > 3$ meV in b) are due to critical current beyond the employed model [44]. c,d) Superconducting order parameter Δ for both samples, obtained with the formula in Eq. 1. The evaluated critical temperature coincides with the emergence of the spectra. The value of the coupling constant $C = \frac{\Delta_{T=0}}{k_B T_c} \gg 1.76$, points to unconventional SC.

Both samples exhibit a much larger $C = \frac{\Delta_{T=0}}{k_B T_c}$ than the one predicted by BCS theory $C = 1.76$. In all our samples studied parameter C varies from 4.5 to 12. It is usually attributed to the unconventional nature of the superconductivity [49].

To further understand the results, transport experiments as a function of temperature and magnetic field were carried out. Fig.3a) shows the evaluated critical magnetic field $\mu_0 H_{c2}$, in both configurations: in-plane $\mu_0 H_{c2\parallel}$ and out-of-plane $\mu_0 H_{c2\perp}$. The measurements were done in a set of magnetic fields while sweeping the temperature in the range 1.5 - 9 K. The critical temperature is attributed to the point where the sample resistance reaches half of the normal state value. The raw data used for determining critical magnetic field are presented in Supplemental Material Fig. S7. The in-plane critical magnetic field exhibits nearly linear behaviour. The out-of-plane critical field, however, follows a power dependence of $H_{c2\perp} \sim (T_c - T)^c$, with $c \approx 1.44$, as shown in Fig.3b). This exponent is reproduced for all sample regions. Having both critical fields determined, we calculate the Cooper pair coherence length $\xi_{\perp(\parallel)}$ within the anisotropic Landau-Ginzburg equations [50, 51]:

$$\mu_0 H_{c\perp} = \frac{\Phi_0}{2\pi\xi_{\perp}^2} \quad ; \quad \mu_0 H_{c\parallel} = \frac{\Phi_0}{2\pi\xi_{\parallel}\xi_{\perp}} \quad (2)$$

The calculated values of coherence lengths do not differ much from dataset to dataset (regions 1-4), and the qualitative temperature trend is conserved. The results are presented in Fig.3c). One can see that ξ_{\perp} never exceeds the thickness of the PbTe or SnTe layer (100 nm), which suggests Cooper pairs are localized at the single interface. On the other hand ξ_{\parallel} is not bound by such a limitation

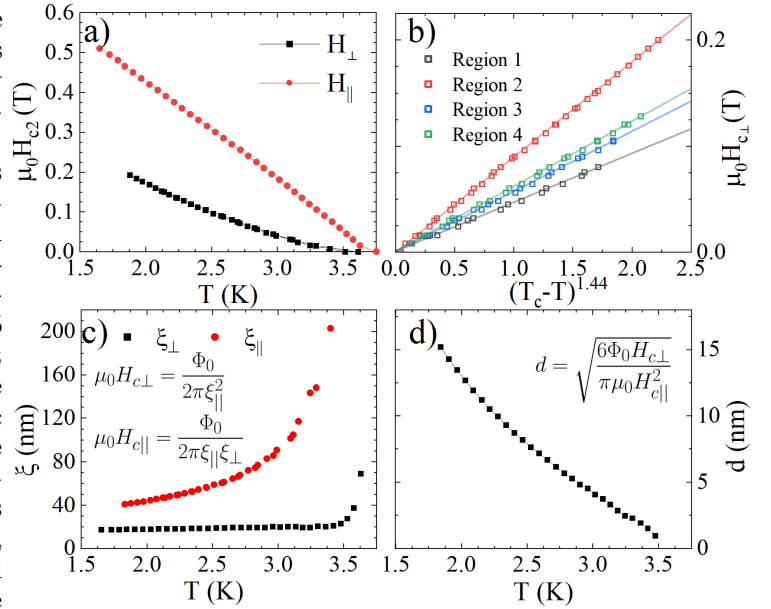


FIG. 3. a) dependence of critical magnetic fields in-plane $\mu_0 H_{c2\parallel}$ and out-of-plane $\mu_0 H_{c2\perp}$ on temperature. b) $\mu_0 H_{c2\perp}$ plotted against $(T_c - T)^{1.44}$ for 4 distinct sample regions, revealing linear dependencies. c) perpendicular ξ_{\perp} and parallel ξ_{\parallel} coherence lengths as a function of temperature obtained from a). d) the thickness of the superconducting layer d determined from the critical magnetic fields. Data presented in panels a), c), and d) are taken from region 2 showcased in b).

and can reach hundreds of nanometers near the critical temperature. At low temperatures, the coherence length approaches a value of a few tens of nm, equal to around

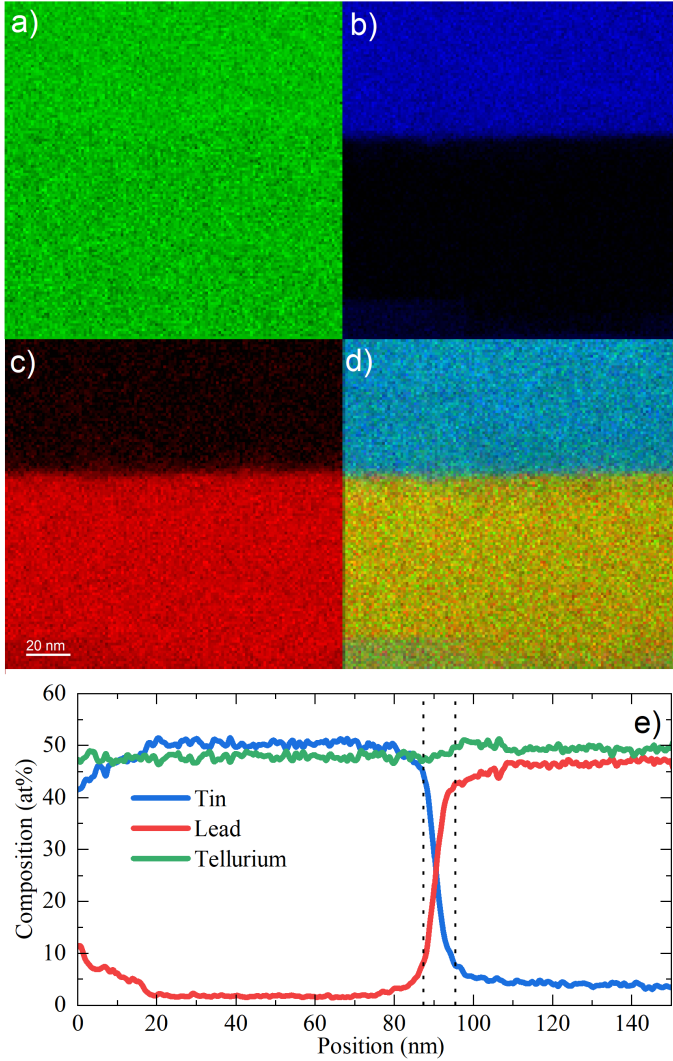


FIG. 4. EDX map of sample cross-sections near the layer interface showing element distribution of tellurium, tin, and lead in figures a)-c), respectively. No precipitates were detected near the interfaces, as shown in d) on an RGB colour map of EDX signal. Panel e) shows averaged atomic compositions along the growth direction.

10 – 20 nm in the case of ξ_{\perp} and 30 – 40 nm in the case of ξ_{\parallel} . Other quantities describing the SC state were evaluated: the effective thickness of the superconducting phase d and a dimensionless factor describing the effective strength of the two-dimensionality of the superconducting layer r [24, 50, 51]:

$$d^2 = \frac{6\Phi_0 H_{c\perp}}{\pi\mu_0 H_{c\parallel}^2} \quad ; \quad r = \frac{4}{\pi} \left(\frac{2\xi_{\perp}}{\lambda} \right)^2 \quad (3)$$

where λ is the distance between SC interfaces ($\lambda \simeq 100$ nm). The calculated d as a function of temperature is presented in Fig.3d). This parameter increases with decreasing temperature. This finding ties nicely with the predictions of Tang and Fu [29]: as stress from interface dislocation relaxes with distance from the interface, the T_c can be spatially dependent along the growth direction. This fact effectively translates to an increase of superconducting phase

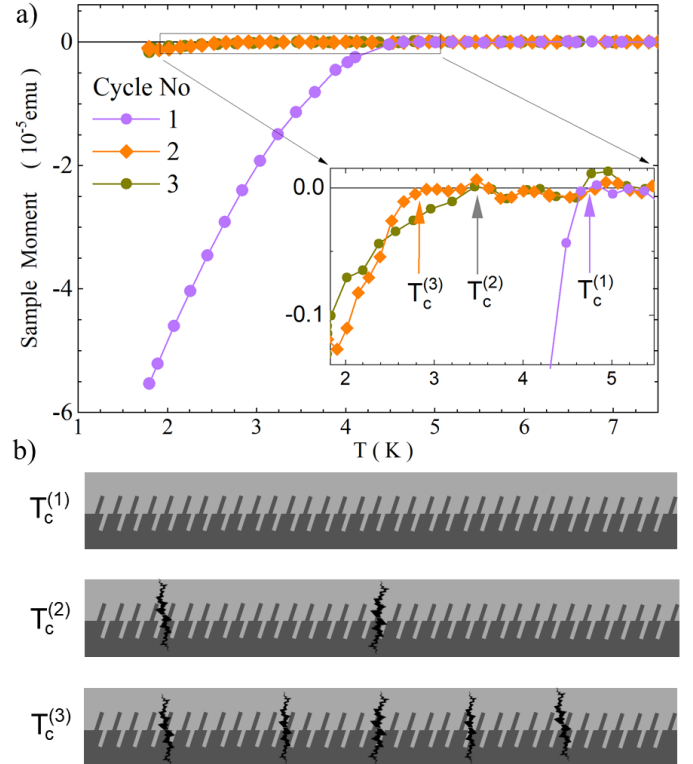


FIG. 5. a) Temperature dependence of magnetization measured in 10 Oe for 3 subsequent cooling processes, showing the Meissner effect fading out. b) Schematically shown degradation of the dislocation grid on the interface, leading to a loss of periodicity and thus breaking down the flatbands.

volume with decreasing temperature and could possibly explain unusual $H_{c\perp}$ behaviour. The interpretation of the r parameter introduced above is as follows: when $r \ll 1$, the SC phase is 2D; when $r \gg 1$, the SC phase is 3D. The evaluated r is consistently smaller than 0.25, explicitly confirming the 2D nature of SC condensate [51].

Close inspection of the interface region with EDX (Energy Dispersive X-rays) spectroscopy presented in Fig. 4 unambiguously shows a clear cut-off between PbTe and SnTe layers without any trace of precipitates. This observation excludes the possibility that the 2D SC condensate is due to the presence of interfacial SC elements. If any precipitates are observed, they are isolated inside the bulk of the layers, as further discussed in supplementary material in Fig. S8. We have also performed magnetization studies using SQUID magnetometry to check how multiple cooling cycles (300 K - 1.8 K) affect the superconductivity. As depicted in Fig. 5a), the Meissner effect is clearly shown. The onset of the diamagnetic signal shifts to lower temperatures, indicating the change in T_c . This change is related to degradation of the periodic dislocation grid in subsequent cooling processes [24], schematically shown in Fig. 5b. If, hypothetically, the superconductivity of the samples originated from grainy precipitates of superconducting elements (Pb or Sn) [52, 53], it should not be sensitive to the thermal cycling of the sample.

This paper presents evidence for spin-triplet pairing in MBE-grown PbTe/SnTe semiconductor superlattices.

Point-contact spectroscopy is used to probe the Andreev reflection with both spin-polarised and -unpolarised electrodes, indicating the p-wave symmetry of the pairing potential. Our findings are in agreement with the Anderson-Brinkman-Morel model of spin-triplet superconductivity. Temperature evolution of the in-plane and out-of-plane critical magnetic fields H_{c2} enabled us to estimate the thickness of the superconducting phase $d \simeq 20\text{nm}$, which is in agreement with the two-dimensional superconductivity induced at the lattice-mismatched interfaces, postulated by Tang and Fu [29]. Our paper offers a new way of designing

a novel flatband systems with material and strain engineering.

ACKNOWLEDGMENTS

This study has been supported by the National Science Centre (Poland) through OPUS (UMO - 2017/27/B/ST3/02470) project and by the Foundation of Polish Science through the IRA Programme co-financed by EU within SG OP.

-
- [1] M. Blamire and J. Robinson, *Superconducting Spintronics and Devices*, edited by A. Narlikar, Vol. 1 (Oxford University Press, 2017).
- [2] J. Linder and J. W. A. Robinson, Superconducting spintronics, *Nature Physics* **11**, 307 (2015).
- [3] C. Beenakker and L. Kouwenhoven, A road to reality with topological superconductors, *Nature Physics* **12**, 618 (2016).
- [4] K. Flensberg, F. Von Oppen, and A. Stern, Engineered platforms for topological superconductivity and Majorana zero modes, *Nature Reviews Materials* **6**, 944 (2021).
- [5] J. Alicea, New directions in the pursuit of Majorana fermions in solid state systems, *Reports on Progress in Physics* **75**, 076501 (2012).
- [6] M. Sato and Y. Ando, Topological superconductors: a review, *Reports on Progress in Physics* **80**, 076501 (2017).
- [7] M. Sato, Topological properties of spin-triplet superconductors and Fermi surface topology in the normal state, *Physical Review B* **79**, 214526 (2009).
- [8] M. Sato, Topological odd-parity superconductors, *Physical Review B* **81**, 220504 (2010).
- [9] Y. Cao, J. M. Park, K. Watanabe, T. Taniguchi, and P. Jarillo-Herrero, Pauli-limit violation and re-entrant superconductivity in moire graphene, *Nature* **595**, 526 (2021).
- [10] M. Oh, K. P. Nuckolls, D. Wong, R. L. Lee, X. Liu, K. Watanabe, T. Taniguchi, and A. Yazdani, Evidence for unconventional superconductivity in twisted bilayer graphene, *Nature* **600**, 240 (2021).
- [11] G. E. Volovik, Flat Band in Topological Matter: Possible Route to Room-Temperature Superconductivity, *Journal of Superconductivity and Novel Magnetism* **26**, 2887 (2013).
- [12] T. T. Heikkilä and G. E. Volovik, Flat Bands as a Route to High-Temperature Superconductivity in Graphite, in *Basic Physics of Functionalized Graphite*, Vol. 244, edited by P. D. Esquinazi (Springer International Publishing, Cham, 2016) pp. 123–143.
- [13] A. Lau, T. Hyart, C. Autieri, A. Chen, and D. I. Pikulin, Designing Three-Dimensional Flat Bands in Nodal-Line Semimetals, *Physical Review X* **11**, 031017 (2021).
- [14] S. Ran, C. Eckberg, Q.-P. Ding, Y. Furukawa, T. Metz, S. R. Saha, I.-L. Liu, M. Zic, H. Kim, J. Paglione, and N. P. Butch, Nearly ferromagnetic spin-triplet superconductivity, *Science* **365**, 684 (2019).
- [15] Y. Shimizu, D. Braithwaite, D. Aoki, B. Salce, and J.-P. Brison, Spin-Triplet p -Wave Superconductivity Revealed under High Pressure in UBe 13, *Physical Review Letters* **122**, 067001 (2019).
- [16] J. Yang, J. Luo, C. Yi, Y. Shi, Y. Zhou, and G.-q. Zheng, Spin-triplet superconductivity in $\text{K}_2\text{Cr}_3\text{As}_3$, *Science Advances* **7**, eabl4432 (2021).
- [17] A. Pustogow, Y. Luo, A. Chronister, Y.-S. Su, D. A. Sokolov, F. Jerzembeck, A. P. Mackenzie, C. W. Hicks, N. Kikugawa, S. Raghu, E. D. Bauer, and S. E. Brown, Constraints on the superconducting order parameter in Sr_2RuO_4 from oxygen-17 nuclear magnetic resonance, *Nature* **574**, 72 (2019).
- [18] D. Abergel, Triplet no more, *Nature Physics* **15**, 1105 (2019).
- [19] C. R. Reeg and D. L. Maslov, Proximity-induced triplet superconductivity in Rashba materials, *Physical Review B* **92**, 134512 (2015).
- [20] T. Nakamura, L. D. Anh, Y. Hashimoto, S. Ohya, M. Tanaka, and S. Katsumoto, Evidence for Spin-Triplet Electron Pairing in the Proximity-Induced Superconducting State of an Fe-Doped InAs Semiconductor, *Physical Review Letters* **122**, 107001 (2019).
- [21] R. Cai, I. Žutić, and W. Han, Superconductor/Ferromagnet Heterostructures: A Platform for Superconducting Spintronics and Quantum Computation, *Advanced Quantum Technologies* **6**, 2200080 (2023).
- [22] K. Murase, S. Ishida, S. Takaoka, T. Okumura, H. Fujiyasu, A. Ishida, and M. Aoki, Superconducting behavior in PbTe/SnTe superlattices, *Surface Science* **170**, 486 (1986).
- [23] N. Y. Fogel, A. S. Pokhila, Y. V. Bomze, A. Y. Sipatov, A. I. Fedorenko, and R. I. Shekhter, Novel Superconducting Semiconducting Superlattices: Dislocation-Induced Superconductivity?, *Physical Review Letters* **86**, 512 (2001).
- [24] N. Y. Fogel, E. I. Buchstab, Y. V. Bomze, O. I. Yuzepovich, A. Y. Sipatov, E. A. Pashitskii, A. Danilov, V. Langer, R. I. Shekhter, and M. Jonson, Interfacial superconductivity in semiconducting monochalcogenide superlattices, *Physical Review B* **66**, 174513 (2002).
- [25] N. Y. Fogel, E. I. Buchstab, Y. V. Bomze, O. I. Yuzepovich, M. Y. Mikhailov, A. Y. Sipatov, E. A. Pashitskii, R. I. Shekhter, and M. Jonson, Direct evidence for interfacial superconductivity in two-layer semiconducting heterostructures, *Physical Review B* **73**, 161306 (2006).
- [26] O. I. Yuzepovich, M. Y. Mikhailov, S. V. Bengus, A. Y. Aladyshkin, E. E. Pestov, Y. N. Nozdrin, A. Y. Sipatov, E. I. Buchstab, and N. Y. Fogel, Interfacial superconductivity in bilayer and multilayer IV–VI semiconductor heterostructures, *Low Temperature Physics* **34**, 985 (2008).
- [27] A. Fedorenko, O. Nashchekina, B. Savitskii, L. Shpakovskaya, O. Mironov, and M. Oszwaldowski, Strain in PbTe/SnTe heterojunctions grown on (001) KCl, *Vacuum* **43**, 1191 (1992).
- [28] S. V. Bengus, A. Y. Sipatov, and S. I. Yuzepovich, Suppression of superconductivity by strong magnetic fields in PbTe/PbS heterostructures with a superconducting interface, *Low Temperature Physics* **39**, 695 (2013).
- [29] E. Tang and L. Fu, Strain-induced partially flat band, helical snake states and interface superconductivity in topolog-

- ical crystalline insulators, *Nature Physics* **10**, 964 (2014).
- [30] T. H. Hsieh, H. Lin, J. Liu, W. Duan, A. Bansil, and L. Fu, Topological crystalline insulators in the SnTe material class, *Nature Communications* **3**, 982 (2012).
- [31] M. A. Silaev and G. E. Volovik, Andreev-Majorana bound states in superfluids, *Journal of Experimental and Theoretical Physics* **119**, 1042 (2014).
- [32] T. T. Heikkilä and G. E. Volovik, Flat bands as a route to high-temperature superconductivity in graphite, in *Springer Series in Materials Science* (Springer International Publishing, 2016) p. 123–143.
- [33] T. Mizushima, Y. Tsutsumi, T. Kawakami, M. Sato, M. Ichioka, and K. Machida, Symmetry-protected topological superfluids and superconductors —from the basics to ^3He , *Journal of the Physical Society of Japan* **85**, 022001 (2016).
- [34] J.-C. He and Y. Chen, Evidence of triplet superconductivity in Bi/Ni bilayers: Theoretical analysis of point contact Andreev reflection spectroscopy results, *Physical Review B* **106**, 224508 (2022).
- [35] R. J. Soulen, M. S. Osofsky, B. Nadgorny, T. Ambrose, P. Broussard, S. F. Cheng, J. Byers, C. T. Tanaka, J. Nowack, J. S. Moodera, G. Laprade, A. Barry, and M. D. Coey, Andreev reflection: A new means to determine the spin polarization of ferromagnetic materials, *Journal of Applied Physics* **85**, 4589 (1999).
- [36] P. W. Anderson and P. Morel, Generalized Bardeen-Cooper-Schrieffer States and Aligned Orbital Angular Momentum in the Proposed Low-Temperature Phase of Liquid He 3, *Physical Review Letters* **5**, 136 (1960).
- [37] A. J. Leggett, A theoretical description of the new phases of liquid ^3He , *Reviews of Modern Physics* **47**, 331 (1975).
- [38] P. W. Anderson and W. F. Brinkman, Anisotropic Superfluidity in ^3He : A Possible Interpretation of Its Stability as a Spin-Fluctuation Effect, *Physical Review Letters* **30**, 1108 (1973).
- [39] D. Feng and G. Jin, *Introduction to condensed matter physics* (World Scientific, Hackensack, NJ, 2005) oCLC: ocm61483641.
- [40] P. Coleman, *Introduction to many body physics* (Cambridge University Press, New York, NY, 2015).
- [41] See supplemental material below for additional data.
- [42] D. Daghero and R. S. Gonnelli, Probing multiband superconductivity by point-contact spectroscopy, *Superconductor Science and Technology* **23**, 043001 (2010).
- [43] H. Wang, L. Ma, and J. Wang, Tip-induced or enhanced superconductivity: a way to detect topological superconductivity, *Science Bulletin* **63**, 1141 (2018).
- [44] G. Sheet, S. Mukhopadhyay, and P. Raychaudhuri, Role of critical current on the point-contact Andreev reflection spectra between a normal metal and a superconductor, *Physical Review B* **69**, 134507 (2004).
- [45] G. He, Z.-X. Wei, J. Brisbois, Y.-L. Jia, Y.-L. Huang, H.-X. Zhou, S.-L. Ni, A. V. Silhanek, L. Shan, B.-Y. Zhu, J. Yuan, X.-L. Dong, F. Zhou, Z.-X. Zhao, and K. Jin, Distinction between critical current effects and intrinsic anomalies in the point-contact Andreev reflection spectra of unconventional superconductors, *Chinese Physics B* **27**, 047403 (2018).
- [46] Quadpy v0.11.3, numerical integration (quadrature, cubature) in python, (2018), doi: 10.5281/ZENODO.1173133.
- [47] C. R. Harris, K. J. Millman, S. J. van der Walt, R. Gommers, P. Virtanen, D. Cournapeau, E. Wieser, J. Taylor, S. Berg, N. J. Smith, R. Kern, M. Picus, S. Hoyer, M. H. van Kerkwijk, M. Brett, A. Haldane, J. F. del Río, M. Wiebe, P. Peterson, P. Gérard-Marchant, K. Sheppard, T. Reddy, W. Weckesser, H. Abbasi, C. Gohlke, and T. E. Oliphant, Array programming with NumPy, *Nature* **585**, 357 (2020).
- [48] M. Zgirski, *Experimental study of fluctuations in ultranarrow superconducting nanowires - LINK*, Ph.D. thesis, University of Jyväskylä, Faculty of Mathematics and Natural Sciences (2008).
- [49] S. Takács, Critical temperature and energy gap in weak- and strong- coupling superconductors with singular density of states, in *Advances in Superconductivity VI*, edited by T. Fujita and Y. Shiohara (Springer Japan, Tokyo, 1994) pp. 63–66.
- [50] A. Wawro, The electron mean free path and superconductivity in Cu/Pb modulated films, *Journal of Physics: Condensed Matter* **5**, 8391 (1993).
- [51] H. Nakajima, M. Ikebe, Y. Muto, and H. Fujimori, Superconducting properties of Mo/Si multilayer films, *Journal of Applied Physics* **65**, 1637 (1989).
- [52] G. P. Mazur, K. Dybko, A. Szczerbakow, J. Z. Domagala, A. Kazakov, M. Zgirski, E. Lusakowska, S. Kret, J. Korczak, T. Story, M. Sawicki, and T. Dietl, Experimental search for the origin of low-energy modes in topological materials, *Physical Review B* **100**, 10.1103/physrevb.100.041408 (2019).
- [53] S. D. Darchuk, L. A. Korovina, F. F. Sizov, T. Dietl, S. Kolesnik, and M. Sawicki, Phase states and magnetic structure of superconducting lead inclusions in a narrow-gap pbte semiconducting host, *Semiconductors* **32**, 700 (1998).

Supplementary Materials for candidate platform for studying flatband-induced spin-triplet superconductivity

P. Sidorczak^{1,2,3,*}, W. Wolkanowicz⁴, A. Kaleta⁴, M. Wójcik⁴, S. Gierałtowska⁴, K. Gas^{4,6}, T. Płociński⁵, R. Minikayev⁴, S. Kret⁴, M. Sawicki^{4,7}, T. Wojtowicz², D. Wasik¹, M. Gryglas-Borysiewicz^{1,†} and K. Dybko^{2,4‡}

¹*Faculty of Physics, University of Warsaw, ul. Pasteura 5, 02-093, Warsaw, Poland*

²*International Research Centre MagTop, Institute of Physics, Polish Academy of Sciences, al. Lotnikow 32/46, 02668, Warsaw, Poland*

³*Center for Quantum Devices, Niels Bohr Institute, University of Copenhagen, Universitetsparken 5, 2100 Copenhagen, Denmark*

⁴*Institute of Physics, Polish Academy of Sciences, al. Lotnikow 32/46, 02668, Warsaw, Poland*

⁵*Faculty of Materials Science and Engineering, Warsaw University of Technology, Wotowska 141, 02-507, Warsaw, Poland*

⁶*Center for Science and Innovation in Spintronics, Tohoku University, Katahira 2-1-1, Aoba-ku, Sendai 980-8577, Japan and*

⁷*Research Institute of Electrical Communication, Tohoku University, Katahira 2-1-1, Aoba-ku, Sendai 980-8577, Japan*

(Dated: June 6, 2024)

CONTENTS

| | |
|--|---|
| A. Structural Characterization | 2 |
| B. Methods of Sample Preparation for Transport Measurements | 4 |
| C. Extended data of PCS characterization | 4 |
| D. Fitting ABM model to PCS data | 6 |
| E. Resistance dependence on temperature and magnetic field | 6 |
| F. Microscopic studies on elemental content of superlattices | 7 |
| G. Record T_c and H_{c2} for PbTe/SnTe superlattice | 8 |
| References | 9 |

* pawel.sidorczak@nbi.ku.dk

† Marta.Gryglas@fuw.edu.pl

‡ dybko@ifpan.edu.pl

A. STRUCTURAL CHARACTERIZATION

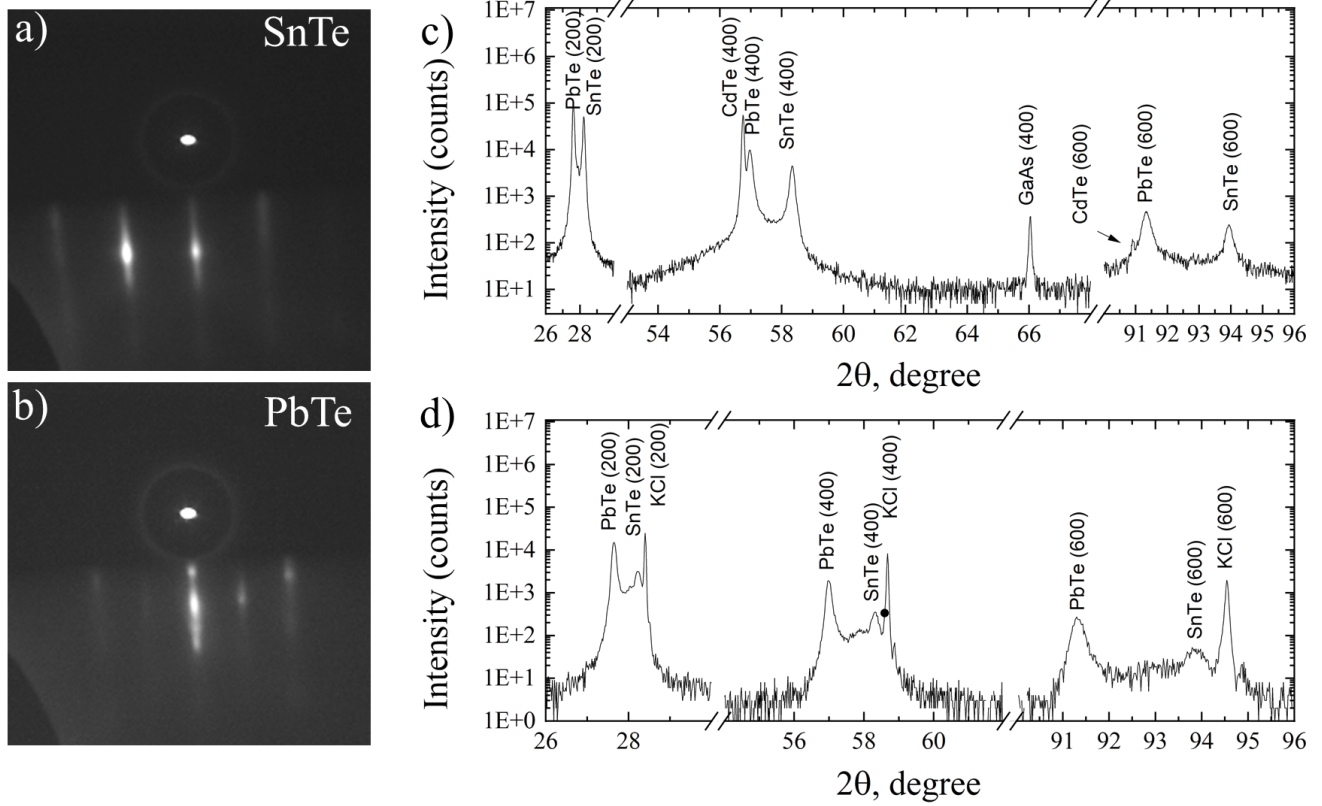


Figure S 1: The sample growth was confirmed to be epitaxial, as can be deduced from RHEED streaky pattern presented in panels a) and b). Typically, PbTe layers were grown in slight tellurium deficiency. The growth was performed from elemental Pb and Te and compound SnTe effusion cell sources. The XRD data in panels c) and d) show the high quality of the samples on both CdTe/GaAs and KCl, respectively.

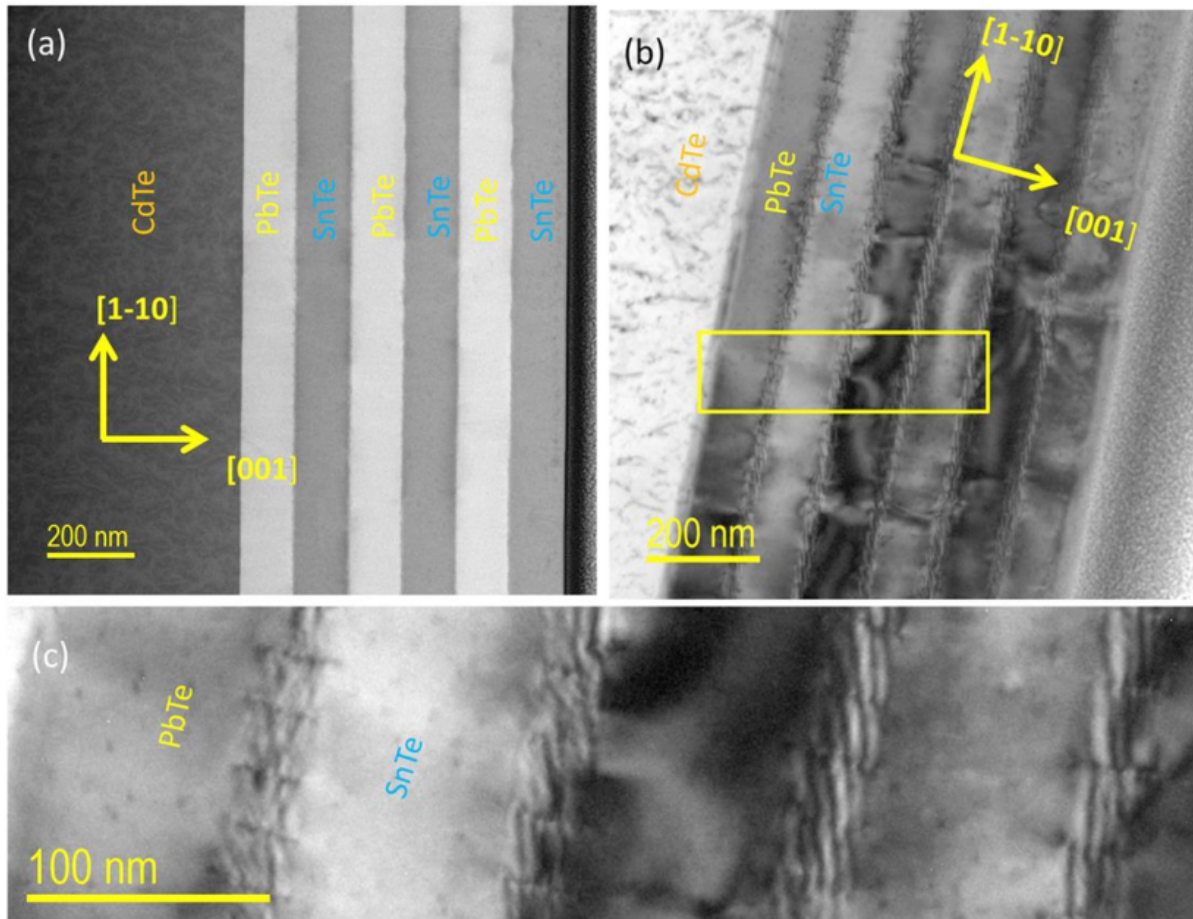


Figure S 2: Thin (transparent for electrons) cross-section was cut from GaAs/CdTe/(PbTe/SnTe) heterostructure with focused ion beam (FIB) and was investigated using a Titan image corrected FEI Titan Cubed 80–300 transmission electron microscope operating at 300 kV. a) STEM Z-contrast image of GaAs/CdTe/(PbTe/SnTe) heterostructure taken in $[110]$ zone axis. In this image, PbTe layer is brighter than SnTe due to its higher averaged Z atomic number. The interfaces, at this scale, seem to be flat, but with a distinct roughness at the level of $\simeq 5$ nm. We do not observe any extended defects in the form of threading dislocations or stacking faults crossing the whole heterostructure. The layers are almost fully relaxed, and the relaxation occurs by the formation of the regular network of misfit dislocations at each interface. b) TEM Bright Field image of misfit dislocations grid at PbTe/SnTe interfaces, c) zoomed part of the yellow frame in panel b) showing diffraction contrast details at the interfaces.

B. METHODS OF SAMPLE PREPARATION FOR TRANSPORT MEASUREMENTS

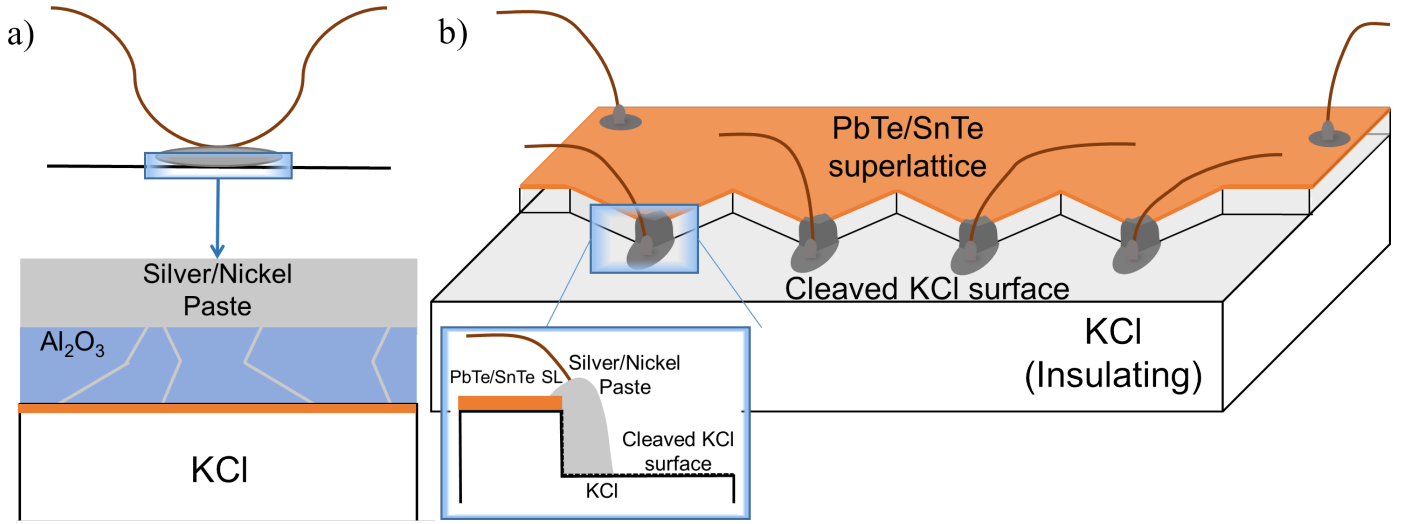


Figure S 3: Two alternative methods for sample preparation techniques used when small contact size is needed. a) Thin Al_2O_3 layer acts as a separator between the contact and the sample. Electron transport is still possible despite the barrier since the coverage is not complete [1]. b) The sample is tailored to form acute triangular edges to reduce the contact area with the adjacent metallic paste.

C. EXTENDED DATA OF PCS CHARACTERIZATION

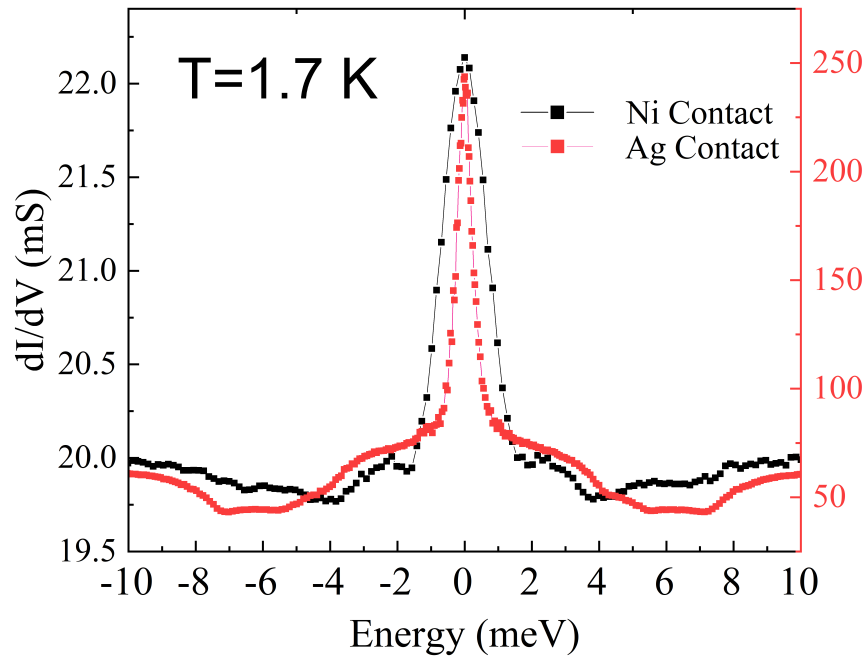


Figure S 4: Result of spin-polarized PCS experiment on contacts obtained with the method presented in Fig.S3 a). The characteristic features of the spectra are preserved, consistent with the results presented in Fig. 1b)

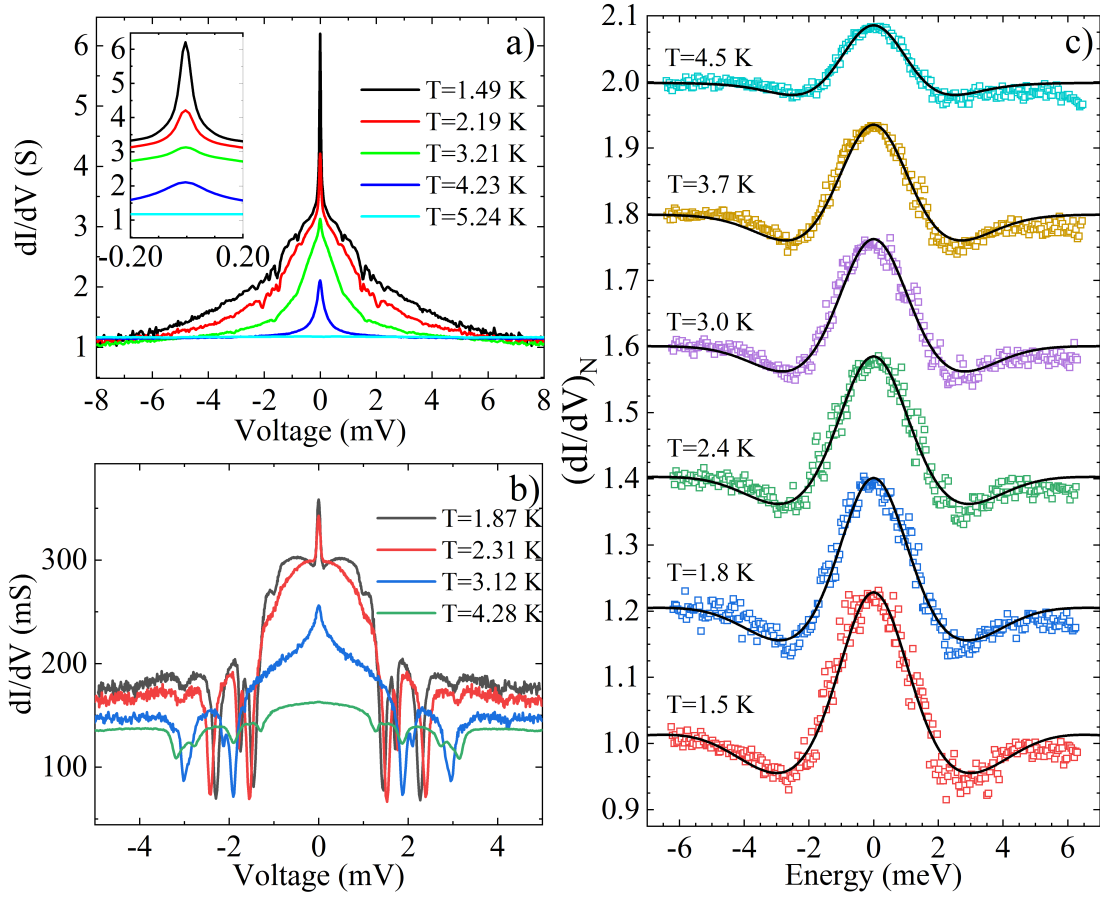


Figure S 5: A choice of different spectra obtained on 3 different samples. Panel a): the least well-resolved SC spectra, showing a thin zero-bias conductance peak (ZBCP) of width of a few microvolts, which is a trivial feature resulting from random interference noise from Josephson junction arrays [2]. Moreover, on the slopes of the peak there is a series of symmetric conductance drops. Most likely, they are caused by critical current breaking down the SC phase. These 2 effects can occur when the sample contact covers multiple superconducting islands in close proximity and the contact conductance is large (above 100 mS). In general, to resolve spectroscopic details of the gap one needs to apply substantial currents, which might exceed the breakdown current. Both of these issues are addressed by decreasing the contact size, as explained in Fig. S3. Panel b): Another PCS spectrum with different features: strong ZBCP mentioned in [2] and a series of critical current dips of the dI/dV . Obtaining any meaningful spectroscopic information is impossible in that case. Contact conductance is of about one order of magnitude smaller in comparison to the data presented in panel a). Panel c): The result obtained on a sample exhibiting the spectra as in panel a) but using a contact separated from the sample with thin Al_2O_3 , as in Fig.3a). The result is fitted with the Anderson-Brinkman-Morel model.

D. FITTING ABM MODEL TO PCS DATA

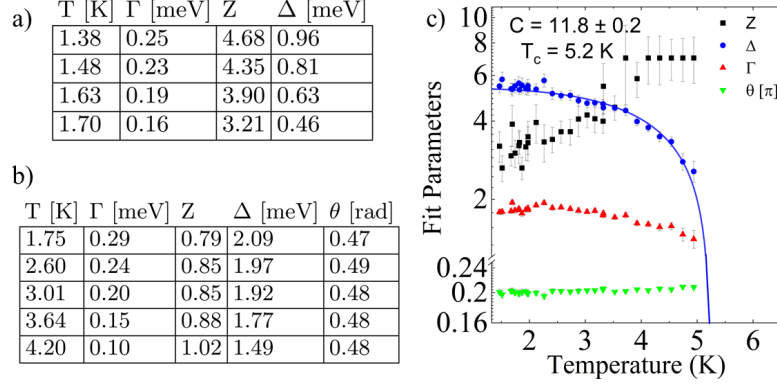


Figure S 6: Fit parameters used to achieve the result presented in Fig 2 a-b) (panel a), Fig. 2 c-d) (panel b), and Fig. S 5c) (panel c)). In all contacts there is a significant change of Γ and Z parameters as a function of temperature, which are the sign of changing contact parameters as a function of temperature. Panel a): The value of fitted θ was kept fixed and has not changed for all fits $\theta = 0.637[\text{rad}] \approx 0.2 \pi[\text{rad}]$. Panel b): none of the fit parameters is fixed. Panel c): Whole dataset of recovered fit parameters extending the ones presented in Fig. S 5c).

E. RESISTANCE DEPENDENCE ON TEMPERATURE AND MAGNETIC FIELD

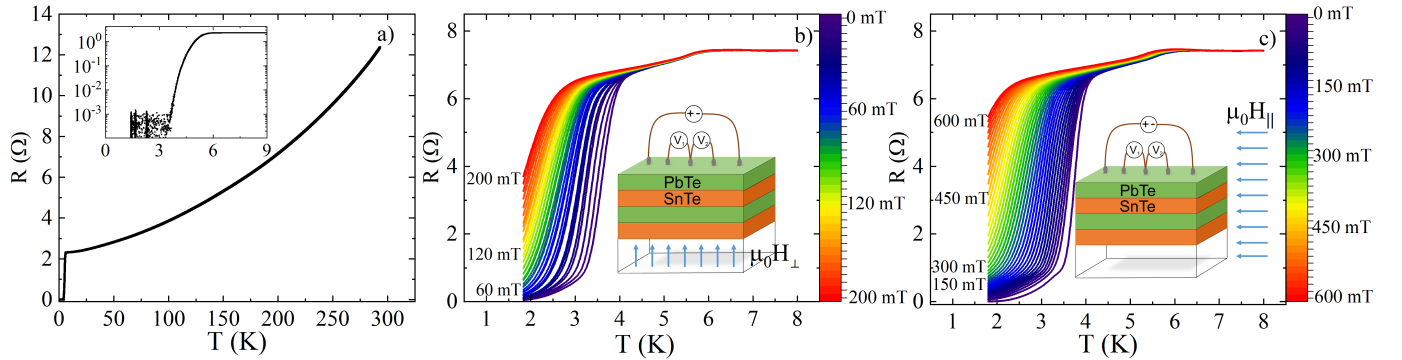


Figure S 7: a) Resistance versus temperature plot taken from 290 down to 1.5 K. The inset presents a clear 3 orders of magnitude resistance drop at the superconducting transition. b-c) The raw data used to extract critical magnetic field presented in Fig.3a) - for the out-of-plane magnetic field $\mu_0 H_{\perp}$ (panel b)) and for the in-plane magnetic field $\mu_0 H_{\parallel}$ (panel c)) configurations. We found that the coherence lengths ξ , dimensionality parameter r , and estimated thickness of the SC layer d obtained using the anisotropic Landau Ginsburg equations do not differ quantitatively from sample to sample and do not depend on whether the SC transition is single or double step.

F. MICROSCOPIC STUDIES ON ELEMENTAL CONTENT OF SUPERLATTICES

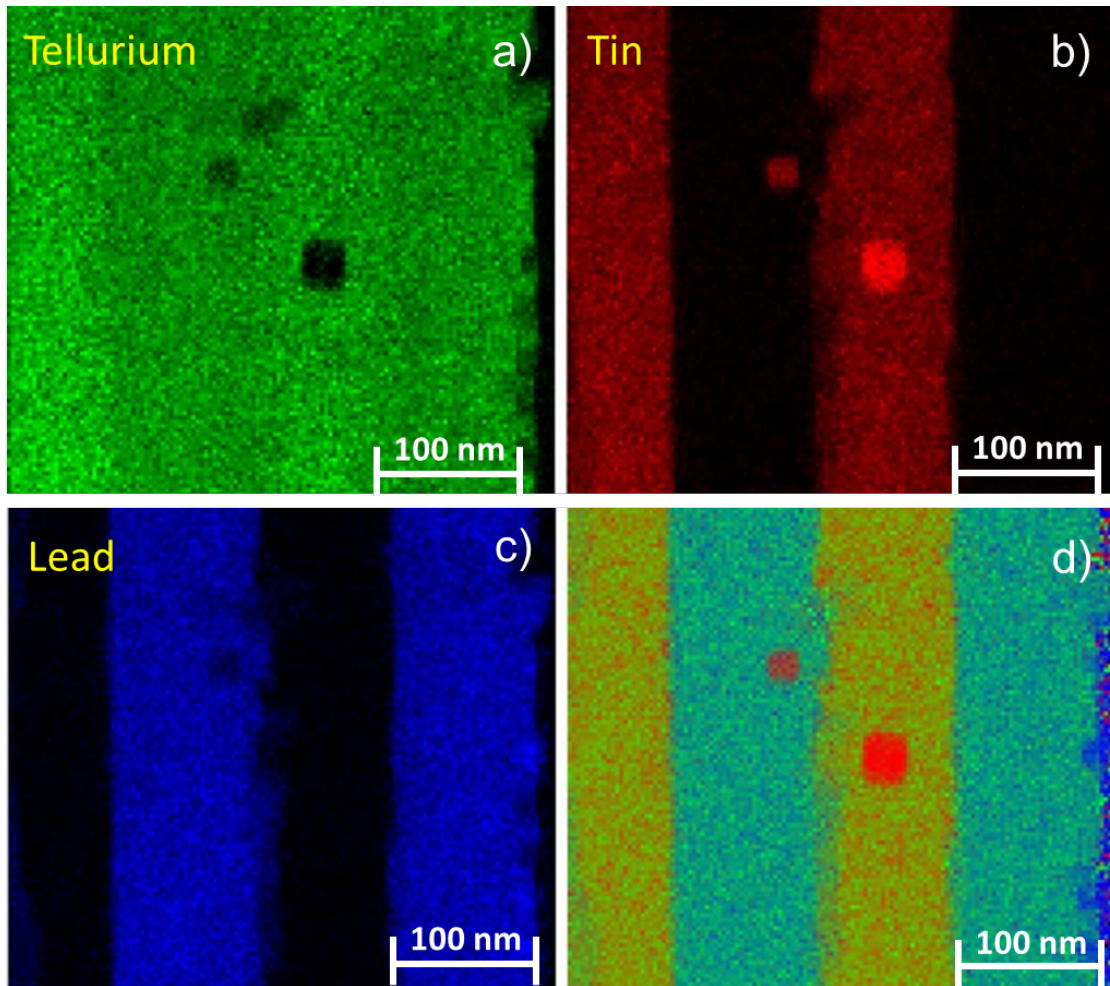


Figure S 8: The EDX imaging performed on sample cross-section for the sample discussed in Fig. 3. Panels a)-c) show elemental distributions of tellurium, tin, and lead, respectively. For this sample, apart from the periodic dislocation grid observed in the TEM images, inclusions / precipitates of Sn were observed, as in panel d) using EDX. However, the concentration of these defects is reasonably small, i.e. the distance between the nearest precipitates is larger than the measured coherence length, and therefore could not have led to a global zero resistance state. Also, despite the imbalance of lead and tellurium fluxes, no lead precipitates have ever been found.

G. RECORD T_c AND H_{c2} FOR PBTE/SNTE SUPERLATTICE

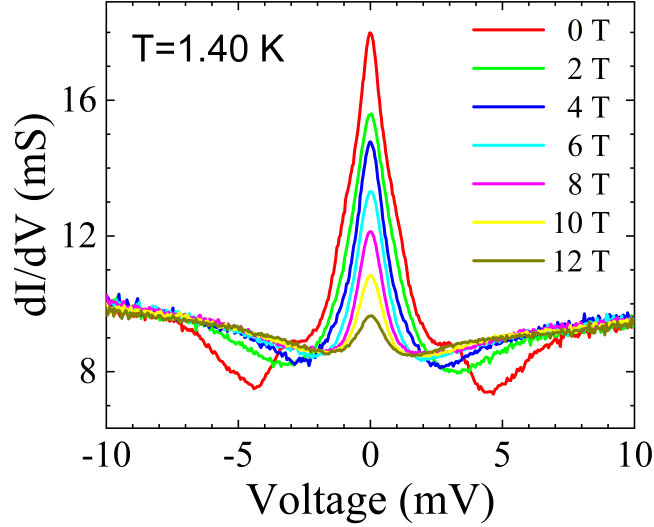


Figure S 9: Collection of PCS data resolved in an external magnetic field. ZBCP dominates the spectra but are wider than in the sets in Fig. 5 (of the range of meV), together with side features, excluding the parasitic effects mentioned above. These results are measured on a nearly fully superconducting sample, so the dips that are disappearing between 0 and 2 Tesla, might be due to the presence of a critical current of the sample (the critical magnetic field in 4-wire resistance measurement did not exceed 500 mT). However, the ZBCP survives in a larger magnetic field, and its features are still well visible at 12 T. If at least a small volume of the sample is still superconducting, it would mean that these results break the Pauli limit, as for this sample, $T_c = 4.75\text{K}$ and Pauli limit states that $\mu_0 H_c = 1.85 T_c \left[\frac{\text{T}}{\text{K}}\right] = 9.25\text{ T}$ [3].

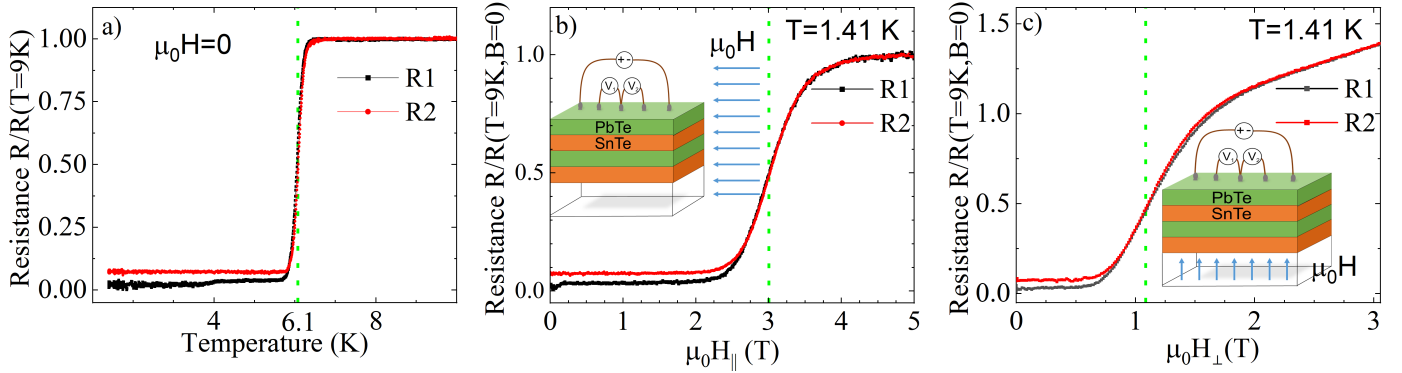


Figure S 10: a) Resistance dependence on temperature for 2 sample regions (R1 and R2, corresponding to 2 voltages V1 and V2 marked on the sample scheme in the inset). Data are normalised to $R(T = 9\text{ K})$ to highlight the most important points. An abrupt superconducting transition is observed, but not complete for R2. b-c) Resistance measurement with out-of-plane and in-plane magnetic fields, respectively, at $T = 1.4\text{ K}$ normalised to the sample resistance at $T = 9\text{ K}$ at zero magnetic field. The evaluated critical magnetic field are $\mu_0 H_{c\perp} \approx 1.1\text{ T}$ $\mu_0 H_{c\parallel} \approx 3.0\text{ T}$, much higher than the known values for superconductors based on IV-VI group materials [4]. For region R1 additional transition is observed at $\mu_0 H < 100\text{ mT}$. Using those values of the estimated critical magnetic fields, the superconductor thickness was calculated to equal roughly $d \approx 22\text{ nm}$ and $r \approx 0.02$ (assuming $\lambda = 100\text{ nm}$). These values stay in good correspondence with the values obtained for the datasets presented in Fig. 3. While it is impossible to use those parameters to confirm that the origin of superconductivity in both cases is the same, a striking similarity can be declared. The measured critical magnetic field does not break the Pauli limit in the weak-coupling superconductor [3] $\mu_0 H_c[\text{T}] = 1.85 T_c[\text{K}]$, where T and K, denote Tesla and Kelvin respectively. This result prompts to ask about to which extent can the critical magnetic field be increased. It is important to stress that the H_c are much larger than the ones observed for the tin precipitates ($T_{c\text{MAX}} \approx 4\text{ K}$, $\mu_0 H_{c\text{MAX}} = 0.2\text{ T}$ [5, 6]).

-
- [1] G. P. Gakis, C. Vahlas, H. Vergnes, S. Dourdain, Y. Tison, H. Martinez, J. Bour, D. Ruch, A. G. Boudouvis, B. Caussat, and E. Scheid, Investigation of the initial deposition steps and the interfacial layer of Atomic Layer Deposited (ALD) Al₂O₃ on Si, *Applied Surface Science* **492**, 245 (2019).
 - [2] G. He, Z.-X. Wei, J. Brisbois, Y.-L. Jia, Y.-L. Huang, H.-X. Zhou, S.-L. Ni, A. V. Silhanek, L. Shan, B.-Y. Zhu, J. Yuan, X.-L. Dong, F. Zhou, Z.-X. Zhao, and K. Jin, Distinction between critical current effects and intrinsic anomalies in the point-contact Andreev reflection spectra of unconventional superconductors, *Chinese Physics B* **27**, 047403 (2018).
 - [3] P. Fulde, High field superconductivity in thin films, *Advances in Physics* **22**, 667 (1973).
 - [4] N. Y. Fogel, E. I. Buchstab, Y. V. Bomze, O. I. Yuzepovich, A. Y. Sipatov, E. A. Pashitskii, A. Danilov, V. Langer, R. I. Shekhter, and M. Jonson, Interfacial superconductivity in semiconducting monochalcogenide superlattices, *Physical Review B* **66**, 174513 (2002).
 - [5] R. Eichele, W. Kern, and R. P. Huebener, Superconductivity of thin films of lead, indium, and tin prepared in the presence of oxygen, *Applied Physics* **25**, 95 (1981).
 - [6] S. Akselrod, M. Pasternak, and S. Bukshpan, Superconductivity and lattice dynamics of granular tin, *Journal of Low Temperature Physics* **17**, 375 (1974).